Microsized single-crystal spinel LAMO for high-power lithium ion batteries synthesized via polyvinylpyrrolidone combustion method

CrossMark

Kehua Dai [a,b], Jing Mao [a,b], Zitao Li [a], Yuchun Zhai [a], Zhihui Wang [b], Xiangyun Song [b], Vince Battaglia [b], Gao Liu [b,*]

[a] School of Materials and Metallurgy, Northeastern University, Shenyang 110004, China
[b] Environmental Energy Technologies Division, Lawrence Berkeley National Laboratory, Berkeley, CA 94720, USA

HIGHLIGHTS

- Microsized single-crystal $Li_{1.08}Mn_{1.89}Al_{0.03}O_4$ (LAMO) was synthesized via polyvinylpyrrolidone (PVP) combustion method.
- The microsized single-crystal LAMO shows excellent cycle performance.
- The microsized single-crystal LAMO exhibits excellent rate and low temperature performance.
- The microsized single-crystal LAMO has high lithium chemical diffusion coefficient.

GRAPHICAL ABSTRACT
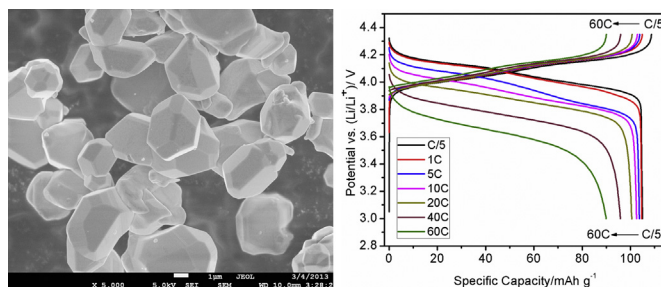
ABSTRACT

Microsized single-crystal $Li_{1.08}Mn_{1.89}Al_{0.03}O_4$ (LAMO) was synthesized via polyvinylpyrrolidone (PVP) combustion method. X-ray diffraction (XRD), scanning electron microscope (SEM) and high-resolution transmission electron microscopy (HRTEM) characterization results indicate that the as-prepared LAMO has good crystallinity, uniform and smooth-surfaced morphology, and very low specific surface area. Galvanostatic charge-discharge tests demonstrate its excellent electrochemical performance. The capacity retentions at 30 °C and 55 °C are 98.8% and 93.3% respectively after 200 cycles at 1 C charge/ discharge rate. Moreover, the LAMO exhibits excellent rate and low temperature performance. Even at high rates of 40 C and 60 C, the as-prepared LAMO are still able to deliver 91.2% and 85.6% capacity relative to the discharge capacity at C/5. The specific discharge capacity at −20 °C is 97.9 mAh g^{-1} which is 93.7% of the capacity discharging at 25 °C. To study the reason of the excellent rate performance, the potential intermittent titration technique (PITT) tests and cyclic voltammetry (CV) measurements were conducted and the lithium chemical diffusion coefficient (D_{Li^+}) was calculated.

Published by Elsevier B.V.

1. Introduction

The rapid development of electric vehicles requires advanced lithium ion batteries with higher power density and longer cycle life. Spinel $LiMn_2O_4$ is at present a very prospective candidate for the cathode (positive electrode) material due to its low cost, good safety, environmental friendliness, and relatively high voltage [1–3]. However, this material shows capacity fading along with cycling due to Jahn–Teller effect [4], oxygen deficiency [5,6], and Mn dissolution [4,7,8]. Li [4,9,10] and Al [11–18] doped $LiMn_2O_4$, abbr. LAMO, has improved cycle performance by lattice modification. Besides doping, to minimize spinel/electrolyte interface is also an important strategy to reduce Mn dissolution and other side

* Corresponding author. Tel.: +1 510 486 7207; fax: +1 510 486 7303.
  E-mail address: Gliu@lbl.gov (G. Liu).

reactions in order to further improve the cycle and storage performance [19,20].

To reduce the spinel/electrolyte interface, the specific surface area must be decreased. Then the particle size should be bigger and the surface should be smoother. Big secondary particles formed by small primary particles are not enough for lower specific surface area [21]. Single-crystal spinel $LiMn_2O_4$ has attracted attention [22–25] in the last decade because this morphology can further reduce the specific surface area. Previous studies show good cycle or storage performance but the rate performance is not good enough. Recently we synthesized microsized $LiNi_{0.5}Mn_{1.5}O_4$ [26] which showed better rate performance than nanosized or sub-microsized materials. Thus, we hypothesize microsized single-crystal spinel LAMO should show excellent rate performance besides excellent cycle performance.

To synthesize microsized single-crystal spinel with excellent rate performance, proper method must be selected and condition should be carefully controlled. The simplest routine is calcined at high temperature (e.g., 1000 °C). However, if precursor is not well mixed, impurities will be easily introduced. In addition, without effective treatment after high temperature calcination, oxygen deficiency will be a serious obstacle for rate and cycle performance.

In this paper, we used a PVP (Polyvinylpyrrolidone)-assisted gel combustion method [26–29] developed by our group to synthesize the microsized single-crystal $Li_{1.08}Mn_{1.89}Al_{0.03}O_4$ (LAMO). PVP can fix metal ion on the macromolecular chain via chelation, so the precursor can be very uniform. The precursor was calcined at high temperature (1000 °C) to produce microsized single crystal. Then a low temperature (700 °C) annealing was performed after mixing a small quantity of lithium compound to lessen oxygen deficiency caused by high temperature [30,31]. The generated microsized single-crystal LAMO not only presented excellent cycle performance but also matched the rate performance of nano particles.

2. Experimental

2.1. Synthesis procedure

The single-crystal spinel LAMO was prepared by the PVP-assisted gel combustion method developed by our group. In detail, $LiOAc·2H_2O$, $Mn(OAc)_2·4H_2O$, $Al(NO_3)_3·9H_2O$ (Li:Mn:Al = 1.08:1.89:0.03), and PVP (the molar ratio of PVP monomer to total metal ions was 2.0) were dissolved in deionized water and pH = 3 was achieved by adding 1:1 HNO_3. The mixture was stirred and dried at 120 °C in air to obtain dried gel. The dried gel was ignited on a hot plate for several minutes to induce a combustion process. The resulting precursor was preheated at 400 °C for 2 h and then calcined at 1000 °C for 6 h in air. The heating rate was 5 °C min^{-1}. After heat treatment, the oven was switched off and the sample was cooled down naturally. 1 wt% Li_2CO_3 was added into the calcined sample and mixed evenly. At last, the mixture was heated at 700 °C for 6 h in air followed by natural cooling.

2.2. Physical characterization

The analysis of the phase purity and the structural characterization were made by X-ray powder diffraction (XRD) using a Bruker D2 PHASER diffractometer equipped with Cu Kα radiation that was operated over a 2θ range of 15–70° in a continuous scan mode with a step size of 0.01°. The lattice parameters were refined by TOPAS software. The particle size and morphology of the samples were examined using a JEOL 7500F scanning electron microscope (SEM). High-resolution transmission electron microscopy (HRTEM) analysis was carried out via a Philips CM200FEG at the

National Center for Electron Microscopy (NCEM) at Lawrence Berkeley National Laboratory and the acceleration voltage was 200 kV. The specific surface area was measured by a Brunauer–Emment–Teller (BET) N_2 adsorption method with a Micromeritics Tristar II 3020 surface area and porosity analyzer. Before the measurement, the sample was heated at 300 °C for 4 h to remove adsorbed water thoroughly.

2.3. Electrochemical tests

All electrochemical performances were evaluated using CR2325 coin cells except for low temperature test in which CR2025 coin cell was used. The coin cells were fabricated with the LAMO cathode, lithium foil anode, 1 mol L^{-1} $LiPF_6$ in 1:1 ethylene carbonate/dimethyl carbonate, and a Celgard 2400 polypropylene separator.

The cathodes were prepared by mixing 88 wt.% active material, 6 wt.% acetylene black (AB) and 6 wt.% polyvinylidene fluoride (PVDF) binder in N-methylpyrrolidone (NMP) to form a slurry. The slurry was stirred for 4 h and then cast onto aluminum foil using a MSK-AFA-III Film Coater (MTI Corporation), dried at 120 °C in air for 2 h and then heated at 130 °C under vacuum for 12 h to prepare the cathode film. The film was punched into discs (diameter = 13 mm) and then pressed at a static pressure of 4–6 MPa. The electrode discs typically had an active material loading of about 5 mg.

The coin cells were assembled in an argon-filled glove box and galvanostatic charge–discharge tests were performed using Maccor 4000 except low temperature test in which LAND CT2001A was used. The potential intermittent titration technique (PITT) test and cyclic voltammetry (CV) measurements were conducted using Bio-Logic VMP-3 multichannel electrochemical Analyzer.

3. Results and discussion

The XRD patterns of the single-crystal spinel LAMO is displayed in Fig. 1. All diffraction peaks can be indexed as a cubic spinel structure and $Fd\overline{3}m$ space group, and no obvious impurity phases are observed in the sample. All of the peaks are narrow and sharp, indicating good crystallinity. The lattice parameter a is 8.2137(8), which is close to other reported values [16,17].

Fig. 2a shows the SEM image of the single-crystal spinel LAMO. The morphology is almost monodispersed truncated-octahedron and the surface of particles is very smooth. The specific surface area is 0.241 ± 0.025 m^2 g^{-1}, which is very low. The sizes of 150
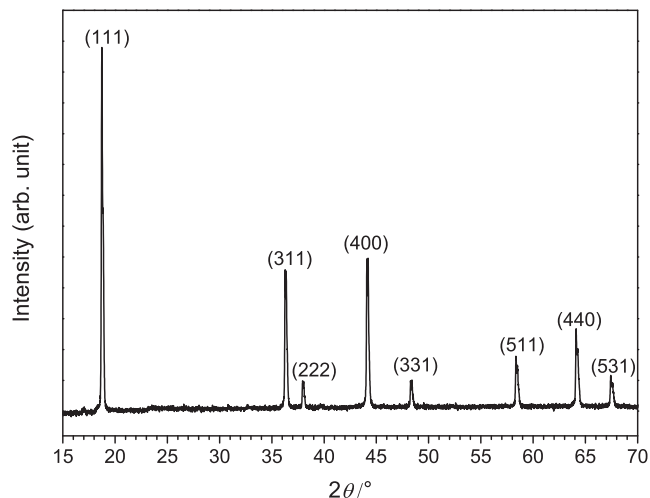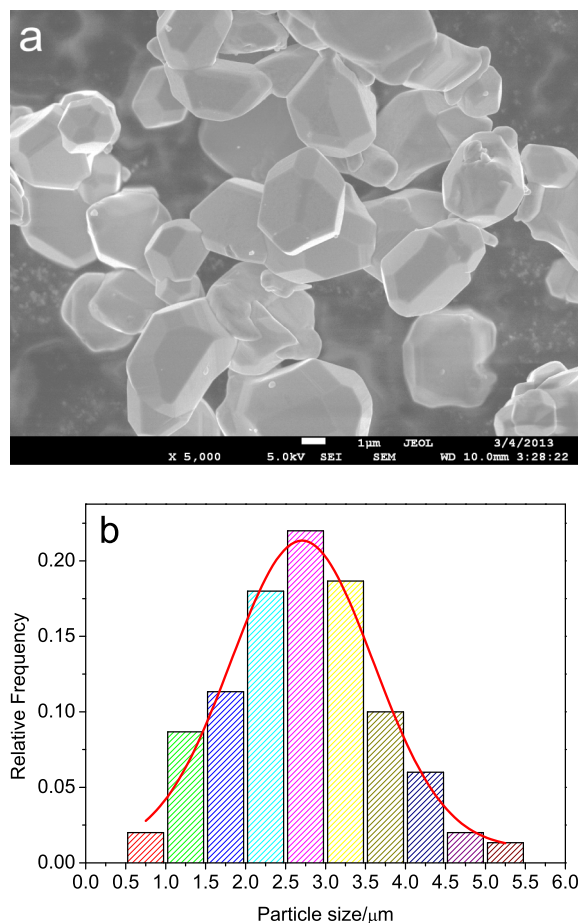

Fig. 1. XRD patterns of the single-crystal spinel LAMO.

Fig. 2. SEM image (a) and particle size distribution (b) of the single-crystal spinel LAMO.

particles are measured in a lower magnification image and the size distribution is calculated and presented in Fig. 2b. The particle size is from 0.5 μm to 5.5 μm and near Gaussian distribution. The mean particle size is 2.7 μm and the standard deviation is 0.94 μm. It is noticed that the morphology of the single-crystal spinel LAMO is very different from that of the similar sample calcined at 700 °C via PVP combustion method [27]. In one of our past works [26], we

studied the influence of temperature on morphology of $LiNi_{0.5}Mn_{1.5}O_4$ and found 1000 °C is a key point for producing single-crystal-like particles via PVP method. At this temperature, the primary particles grow quickly and merge together then form big particles. The big particles have smaller surface energy so they tend to be monodispersed. The big particles, smooth surface, and low specific surface area should decrease Mn dissolution and improve cycle performance.

HRTEM (Fig. 3) was carried out to confirm that the LAMO was constituted by single crystals. The lattice in Fig. 3a has 0.47 nm d-value which corresponds to the (111) plane. Fig. 3b shows right-angled intersection of (220) and ($\bar{2}$20) plane with 0.29 nm d-value. The HRTEM images indicate clearly that the as-prepared LAMO has ordered lattice and single-crystal structure [32]. The ordered lattice will favor the intercalation and deintercalation of Li^+ ion, then the rate performance should be good.

Fig. 4 shows the cycle performance of the as-prepared single-crystal LAMO at 30 °C and 55 °C. The capacity retentions at 30 °C and 55 °C are 98.8% and 93.3% respectively after cycling 200 cycles at 1 C charge/discharge rate. The corresponding capacity decaying rate is calculated as 0.006% and 0.034% per cycle respectively at 30 °C and 55 °C. The average coulombic efficiency at 30 °C and 55 °C is 99.86% and 99.68% respectively. This means the side reactions taking place in the positive solid and electrolyte interface are rather small. High temperature heating (>1000 °C) is critical for particles growing into microsized particles with smooth and small-area surface; Annealing at 700 °C by adding small extra lithium source can help reconstructing the surface crystal lattice (deleting oxygen defects) and ensure the accurate chemical composition; Besides, doping element such as lithium and aluminum can strengthen the spinel manganese oxide structure and reduce the lattice volume change during lithium de/insertion. All the above reasons have contributions to the impressively excellent cycle performance of the single-crystal LAMO.

The as-prepared LAMO was tested at various C rates. The cell was charged and discharged at C/5 for 3 cycles, then it was charged at 1 C and discharged at 1 C, 5 C, 10 C, 20 C, 40 C and 60 C for 5 cycles each. As shown in Fig. 5a, the charge and discharge capacities at C/2 are 108.7 mAh g^{-1} and 105.0 mAh g^{-1}, which are similar to other reported Li and Al doping spinel [16,17]. The coulombic efficiency of the first cycle is 96.6%. The charge and discharge curves do not show any 3.2 V plateau which relates to oxygen deficiency [33]. The two plateaus at 4.0 V and 4.15 V are not easily distinguished due to Li and Al doping.
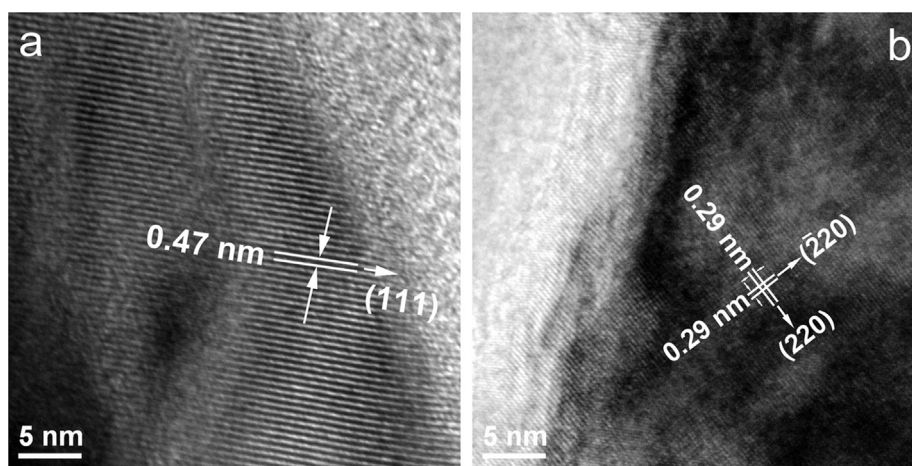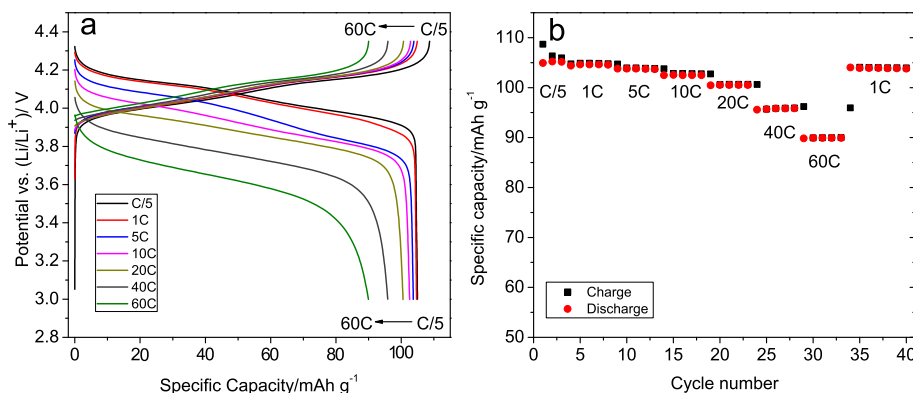

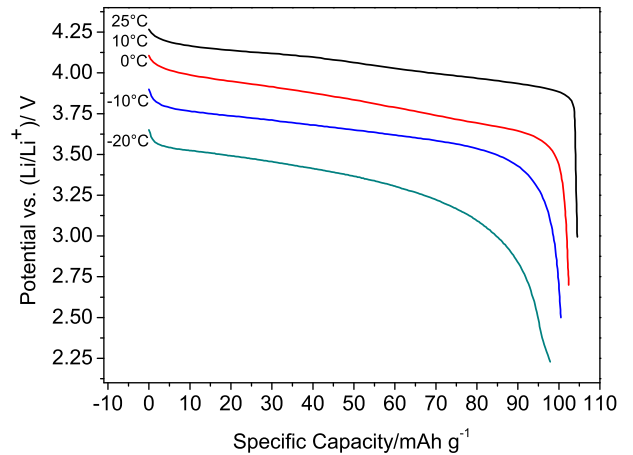**Fig. 3.** HRTEM images of the single-crystal spinel LAMO.
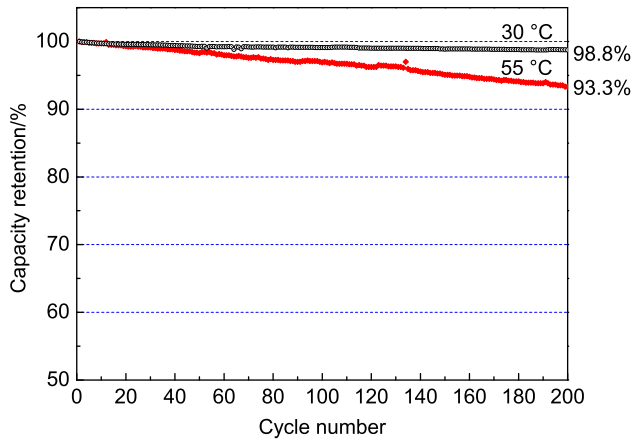
Fig. 4. Cycle performance of the single-crystal spinel LAMO at 30 °C and 55 °C. The charge and discharge rate is 1 C.

At 1 C, 5 C, 10 C, 20 C, 40 C and 60 C, the discharge capacities are 104.7 mAh g^{-1}, 103.7 mAh g^{-1}, 102.5 mAh g^{-1}, 100.5 mAh g^{-1}, 95.8 mAh g^{-1}, and 89.9 mAh g^{-1}, respectively. Even at 40 C and 60 C, the as-prepared LAMO are still able to deliver 91.2% and 85.6% capacity relative to discharge capacity at C/5. Furthermore, it can be seen from Fig. 5b that the capacity variation is small at every rate. This rate performance is better than previous results [16,24,34—37] including the LMO nano-flakes synthesized via PVP combustion method [27]. The possible reason of the excellent rate performance is that in the single crystal Li-ion does not need to across grain boundary, so the Li-ion diffusion coefficient in this single crystal LAMO should be higher than the material composed by aggregate of small particles. Moreover, it should be noticed that the percentage of conductive additive in this electrode is 6%, which is lower than that in many literature [16,24,34—36]. The easy homogeneous mixing of monodispersed micro particles allows lower amount of conductive additive.

Low temperature performance is important for EVs and HEVs in winter or high-latitudinal areas. The single-crystal spinel LAMO also has excellent low temperature performance. Fig. 6 shows discharge profiles of the single-crystal spinel LAMO at different temperatures. Although the voltage plateaus decrease much because the electrolyte was not optimized specifically for low temperature applications, the discharge capacity still remains high. At 10 °C, 0 °C, −10 °C and −20 °C, the specific discharge capacity are 104.1 mAh g^{-1}, 102.4 mAh g^{-1}, 100.5 mAh g^{-1}, 97.9 mAh g^{-1} which are 99.6%, 98.0%, 96.2%, 93.7% of the capacity discharging at 25 °C. The high capacity retention at low temperature may profit from unhindered Li-ion diffusion in the single-crystal LAMO.
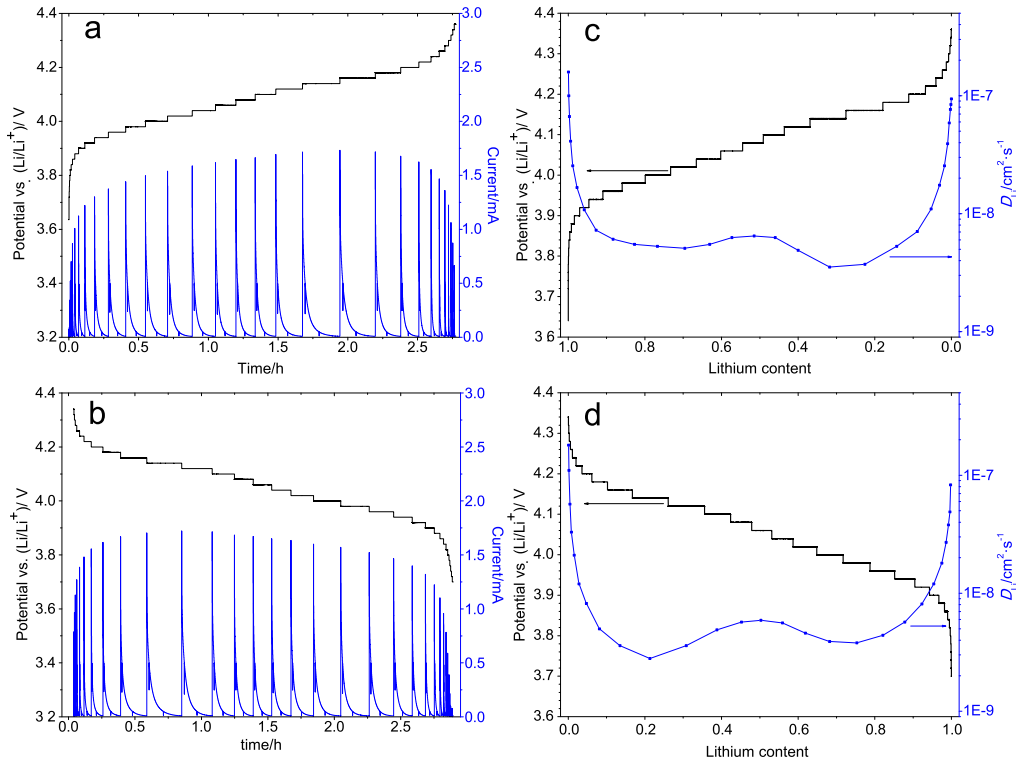

Fig. 6. Discharge profiles of the single-crystal spinel LAMO at different temperature. The charge processed were always performed at room temperature. The charge and discharge rate was 1 C.

It is generally recognized that the rate performance of cathode materials is governed by the diffusion of lithium ion in solid phase [38]. To further understand the reason of the good rate performance of the single-crystal spinel LAMO, the lithium chemical diffusion coefficient (D_{Li^+}) was determined by potential intermittent titration technique (PITT). In the PITT experiments, a small potential step size (20 mV) and a low enough cutoff current (C/50) were adopted to ensure the equilibrium states were achieved at every potential step. Then the lithium chemical diffusion coefficient, D_{Li^+}, can be calculated from the slope of the linear region in the ln $I(t)$ vs. t plot, as defined in equation (1) [39]:

$$D_{Li^+} = -\frac{d\ln(I)}{dt}\frac{4L^2}{\pi^2} \tag{1}$$

where I is the current in the potential step and L is the thickness of the electrode (13 μm). The values of D_{Li^+} measured from PITT and the potential plotted with lithium content are shown in Fig. 7. The lithium diffusion values vary considerably with concentration from 2.8×10^{-9} cm^2 s^{-1} to 1.8×10^{-7} cm^2 s^{-1}. Two diffusion minima are observed for both charge and discharge, but the fluctuation of D_{Li^+} is not as big as stoichiometric LiMn$_2$O$_4$. It should be noticed that these are apparent diffusion coefficient values of solvated lithium ions, which are affected by many factors such as effective surface area of porous electrode; particle size and orientation; diffusion pathway radius; pore size; influence of mobility in the liquid state [40], so the intrinsic lithium chemical diffusion coefficient should

Fig. 5. Charge and discharge profiles (a) and specific capacity vs. cycle number plot (b) of the single-crystal spinel LAMO at different C rates.

Fig. 7. PITT and lithium chemical diffusion coefficient profiles of the single-crystal spinel LAMO. a. Potential vs. (Li/Li$^+$) and current response during charge; b. Potential vs. (Li/Li$^+$) and current response during discharge. c. Potential vs. (Li/Li$^+$) and corresponding lithium chemical diffusion coefficient during charge. d. Potential vs. (Li/Li$^+$) and corresponding lithium chemical diffusion coefficient during discharge.

be higher. By comparison, they are higher than the previous results [14,23,41,42]. The high value and relatively small change of lithium chemical diffusion coefficient result in quick and stable Li$^+$ intercalation and deintercalation, so the single-crystal spinel LAMO has very excellent rate performance.

To further study the electrochemical characteristics of the single-crystal spinel LAMO as a cathode for lithium-ion battery, we conducted a series of cyclic voltammetry measurements. The results are shown in Fig. 8. The cell was cycled between 3.0 V and 4.3 V at scan rates of 0.1 mV s^{-1}, 0.2 mV s^{-1}, 0.3 mV s^{-1}, 0.4 mV s^{-1}, and between 3.0 V and 4.5 V at scan rate of 0.5 mV s^{-1}. There is no any peak at 3.2 V, confirming that the sample has no oxygen deficiency. Two couples of redox current peaks are observed at 4.05/4.17 V and 3.98/4.11 V when the scan rate is 0.1 mV s^{-1}. The anodic peaks are lower and the cathodic peaks are higher than the previous result [16], though in which the scan rate was lower (0.058 mV s^{-1}), indicating better charge–discharge reversibility. The lithium chemical diffusion coefficient is also calculated from the CV results. For a reversible reaction relating Li-ion diffusion behavior, the lithium chemical diffusion coefficient (D_{Li^+}) can be determined on the basis of the following Randles–Sevcik equation [43]:

$$i_p = 0.4463 n^{\frac{3}{2}} F^{\frac{3}{2}} C_{Li} A R^{-\frac{1}{2}} T^{-\frac{1}{2}} D_{Li}^{\frac{1}{2}} v^{\frac{1}{2}} \tag{2}$$

At 30 °C:

$$i_p = \left(2.67 \times 10^5\right) n^{\frac{3}{2}} C_{Li} A D_{Li}^{\frac{1}{2}} v^{\frac{1}{2}} \tag{3}$$

where i_p is the peak current value (A), n is the number of electrons per reaction species (for Li$^+$ $n = 1$), C_{Li} is the bulk concentration of lithium-ion in the electrode (0.0238 mol cm^{-3} for LiMn$_2$O$_4$ derived

from the theoretical density of 4.3 g cm^{-3}), A is the surface area of electrode (here is 1.26 cm^2), D_{Li} is the lithium chemical diffusion coefficient (cm^2 s^{-1}), and v is the scan rate (V s^{-1}). From the slope of linear fit of the peak current (i_p) vs. the square root of the scan rates ($v^{1/2}$) in Fig. 8, the D_{Li^+} of the single-crystal spinel LAMO is calculated as 4.9×10^{-9} cm^2 s^{-1}, which consists with the result from PITT.

With the calculated lithium chemical diffusion coefficient, the diffusion time of Li$^+$ in the particles can be estimated using $L^2 = Dt$. The upper limit of the particle size in Fig. 2b is about 5.5 μm, so $L \approx 5.5 \times 10^{-4}$ cm. Thus, Li$^+$ can migrate from one side to another
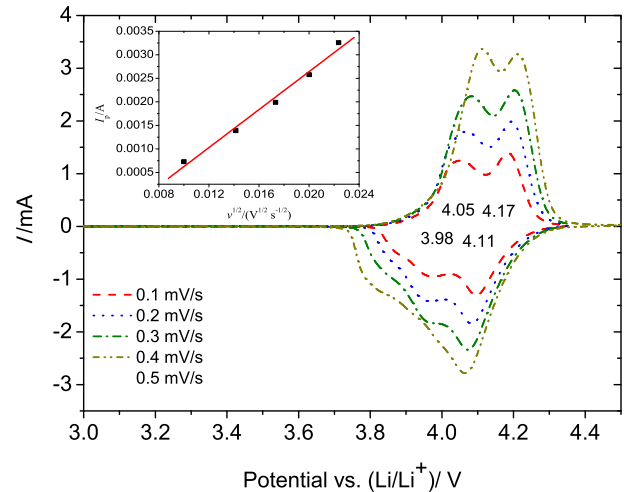
Fig. 8. CV profiles of the single-crystal spinel LAMO.

side of the biggest particles in 1 min with $D_{Li^+} = 4.9 \times 10^{-9}$ cm^2 s^{-1}, which corresponds to 60 C and agrees the result of rate test.

4. Conclusion

Microsized single-crystal Li$_{1.08}$Mn$_{1.89}$Al$_{0.03}$O$_4$ (LAMO) was synthesized via PVP combustion method. It shows good crystallinity, uniform and smooth-surfaced morphology, and very low specific surface area. The single-crystal LAMO with a mean particle size of 2.71 μm has excellent cycle performance. The capacity retentions at 30 °C and 55 °C are 98.8% and 93.3% respectively after cycling 200 cycles at 1 C charge/discharge rate. The low temperature performances of LAMO are also excellent. Even at 40 C and 60 C, the as-prepared LAMO are still able to deliver 91.2% and 85.6% capacity relative to discharging at C/5. At −20 °C, the specific discharge capacity and its retention are 97.9 mAh g^{-1} and 93.7%. The excellent rate and low temperature performance due to the high lithium chemical diffusion coefficient (D_{Li^+}).

Acknowledgment

References

[1] A. Manthiram, J. Phys. Chem. Lett. 2 (2011) 176–184.
[2] J.M. Tarascon, M. Armand, Nature 414 (2001) 359–367.
[3] J.M. Tarascon, E. Wang, F.K. Shokoohi, W.R. Mckinnon, S. Colson, J. Electrochem. Soc. 138 (1991) 2859–2864.
[4] R.J. Gummow, A. Dekock, M.M. Thackeray, Solid State Ionics 69 (1994) 59–67.
[5] X.Q. Wang, H. Nakamura, M. Yoshio, J. Power Sources 110 (2002) 19–26.
[6] B.H. Deng, H. Nakamura, M. Yoshio, J. Power Sources 180 (2008) 864–868.
[7] Y.Y. Xia, Y.H. Zhou, M. Yoshio, J. Electrochem. Soc. 144 (1997) 2593–2600.
[8] W. Choi, A. Manthiram, J. Electrochem. Soc. 153 (2006) A1760–A1764.
[9] Y.Y. Xia, T. Sakai, T. Fujieda, X.Q. Yang, X. Sun, Z.F. Ma, J. McBreen, M. Yoshio, J. Electrochem. Soc. 148 (2001) A723–A729.
[10] Y.J. Shin, A. Manthiram, Electrochem. Solid-State Lett. 5 (2002) A55–A58.
[11] L.F. Xiao, Y.Q. Zhao, Y.Y. Yang, Y.L. Cao, X.P. Ai, H.X. Yang, Electrochim. Acta 54 (2008) 545–550.
[12] K. Ariyoshi, E. Iwata, M. Kuniyoshi, H. Wakabayashi, T. Ohzuku, Electrochem. Solid-State Lett. 9 (2006) A557–A560.
[13] G.G. Amatucci, N. Pereira, T. Zheng, J.M. Tarascon, J. Electrochem. Soc. 148 (2001) A171–A182.
[14] S.T. Myung, S. Komaba, N. Kumagai, J. Electrochem. Soc. 148 (2001) A482–A489.
[15] F. Le Cras, D. Bloch, M. Anne, P. Strobel, Solid State Ionics 89 (1996) 203–213.
[16] M. Prabu, M.V. Reddy, S. Selvasekarapandian, G.V.S. Rao, B.V.R. Chowdari, Electrochim. Acta 88 (2013) 745–755.
[17] D.-J. Lee, K.-S. Lee, S.-T. Myung, H. Yashiro, Y.-K. Sun, J. Power Sources 196 (2011) 1353–1357.
[18] Y. Shin, A. Manthiram, J. Electrochem. Soc. 151 (2004) A204–A208.
[19] G. Amatucci, A. Du Pasquier, A. Blyr, T. Zheng, J.M. Tarascon, Electrochim. Acta 45 (1999) 255–271.
[20] G.G. Amatucci, C.N. Schmutz, A. Blyr, C. Sigala, A.S. Gozdz, D. Larcher, J.M. Tarascon, J. Power Sources 69 (1997) 11–25.
[21] Y. Shin, A. Manthiram, J. Power Sources 126 (2004) 169–174.
[22] J. Akimoto, Y. Takahashi, N. Kijima, Electrochem. Solid-State Lett. 8 (2005) A361–A364.
[23] K. Dokko, M. Nishizawa, M. Mohamedi, M. Umeda, I. Uchida, J. Akimoto, Y. Takahashi, Y. Gotoh, S. Mizuta, Electrochem. Solid-State Lett. 4 (2001) A151–A153.
[24] Y.L. Ding, J. Xie, G.S. Cao, T.J. Zhu, H.M. Yu, X.B. Zhao, J. Phys. Chem. C 115 (2011) 9821–9825.
[25] M.W. Raja, S. Mahanty, R.N. Basu, Solid State Ionics 180 (2009) 1261–1266.
[26] J. Mao, K.H. Dai, Y.C. Zhai, Electrochim. Acta 63 (2012) 381–390.
[27] J. Mao, K.H. Dai, Y.C. Zhai, Acta Phys-Chim. Sin. 28 (2012) 349–354.
[28] J. Mao, K.H. Dai, W.B. Luo, Y.C. Zhai, in: The 15th International Meeting on Lithium Batteries, Montréal, Canada, 2010.
[29] K.H. Dai, J. Mao, Y.C. Zhai, Acta Phys-Chim. Sin. 26 (2010) 2130–2134.
[30] Y.G. Xia, Q. Zhang, H.Y. Wang, H. Nakamura, H. Noguchi, M. Yoshio, Electrochim. Acta 52 (2007) 4708–4714.
[31] B.H. Deng, H. Nakamura, Q. Zhang, M. Yoshio, Y.Y. Xia, Electrochim. Acta 49 (2004) 1823–1830.
[32] L. He, S.C. Zhang, X. Wei, Z.J. Du, G.R. Liu, Y.L. Xing, J. Power Sources 220 (2012) 228–235.
[33] M. Yoshio, H. Noguchi, H.Y. Wang, X.Q. Wang, J. Power Sources 154 (2006) 273–275.
[34] Z.H. Li, J. Yang, J.L. Wang, J.J. Tang, G.T. Lei, Q.Z. Xiao, Microporous Mesoporous Mater. 162 (2012) 44–50.
[35] Y.L. Ding, J.A. Xie, G.S. Cao, T.J. Zhu, H.M. Yu, X.B. Zhao, Adv. Funct. Mater. 21 (2011) 348–355.
[36] E. Hosono, T. Kudo, I. Honma, H. Matsuda, H.S. Zhou, Nano Lett. 9 (2009) 1045–1051.
[37] Y. Shin, A. Manthiram, Electrochem. Solid-State Lett. 6 (2003) A34–A36.
[38] L. Xiao, Y.L. Guo, D.Y. Qu, B.H. Deng, H.X. Liu, D.P. Tang, J. Power Sources 225 (2013) 286–292.
[39] C.J. Wen, B.A. Boukamp, R.A. Huggins, W. Weppner, J. Electrochem. Soc. 126 (1979) 2258–2266.
[40] J.O. Besenhard, J. Heydecke, E. Wudy, H.P. Fritz, W. Foag, Solid State Ionics 8 (1983) 61–71.
[41] J.L. Wang, Z.H. Li, J. Yang, J.J. Tang, J.J. Yu, W.B. Nie, G.T. Lei, Q.Z. Xiao, Electrochim. Acta 75 (2012) 115–122.
[42] S.R. Li, Y. Qiao, Y. Sun, S.Y. Ge, Y.M. Chen, I. Lieberwirth, Y. Yu, C.H. Chen, Electrochim. Acta 81 (2012) 191–196.
[43] Rs Nicholso, Anal. Chem. 37 (1965) 1351–1355.